Mineralogical Magazine, December 2017, Vol. 81(6), pp. 1439–1456

The determination of the Sb/As content in natural tetrahedrite–tennantite and bournonite–seligmannite solid solution series by Raman spectroscopy

A. I. Apopei[1,*], G. Damian[1,2], N. Buzgar[1], A. Buzatu[1], P. Andráš[3] and S. Milovska[4]

[1] "Alexandru Ioan Cuza" University of Iaşi, Faculty of Geography and Geology, Department of Geology, 20A Carol I Blv., 700505 Iaşi, Romania
[2] Technical University of Cluj-Napoca, North University Center of Baia Mare, 62A Dr. Victor Babeş Street, 430083 Baia Mare, Romania
[3] Faculty of Natural Sciences, Matej Bel University, Tajovského 40, 974 01 Banská Bystrica; Slovakia
[4] Geological Institute, Slovak Academy of Sciences, Severná 5, 974 01 Banská Bystrica, Slovakia

[*Received 9 November 2016; Accepted 25 January 2017; Associate Editor: Giancarlo Della Ventura*]

ABSTRACT

Natural samples containing tetrahedrite–tennantite, bournonite–seligmannite and geocronite–jordanite from the Coranda-Hondol ore deposit, Romania, were investigated by Raman spectroscopy to determine its capability to provide estimates of solid solutions in three common and widespread sulfosalt mineral series. Raman measurements were performed on extended solid solution series (Td_1 to Td_{97}, Bnn_{25} to Bnn_{93} and Gcn_{24} to Gcn_{67}, apfu). The tetrahedrite–tennantite and bournonite–seligmannite solid solution series show strong correlations between spectroscopic parameters (position, relative intensity and shape of the Raman bands) and the Sb/(Sb+As) content ratio, while Raman spectra of geocronite–jordanite shows no evolution of Raman bands. In order to simplify the method used to estimate the Sb/(Sb+As) content ratio in tetrahedrite–tennantite and bournonite–seligmannite series, several linear equations of the first-order polynomial fit were obtained. The results are in good agreement with electron microprobe data. Moreover, a computer program was developed as an analytical tool for a fast and accurate determination of Sb/(Sb+As) content ratio by at least one spectroscopic parameter. These results indicate that Raman spectroscopy can provide direct information on the composition and structure of the tetrahedrite–tennantite and bournonite–seligmannite series.

Keywords: Raman spectroscopy, tetrahedrite, tennantite, bournonite, seligmannite, geocronite, jordanite, Sb/(Sb+As) content, sulfosalts.

Introduction

Sulfosalts are a large group of compound semiconductors comprising more than 200 valid mineral species (Moëlo *et al.*, 2008). Sulfosalts have diverse applications in economic, scientific and technical fields, including: photovoltaic and thermoelectric energy conversion, catalysis, X-Ray detectors, etc. (Dittrich *et al.*, 2009; Chetty *et al.*, 2015).

*E-mail: andrei.apopei@uaic.ro
https://doi.org/10.1180/minmag.2017.081.008

Minerals of the tetrahedrite–tennantite series ($(Cu,Ag)_{10}(Fe,Zn)_2Sb_4S_{13}$–$(Cu,Ag)_{10}(Fe,Zn)_2As_4S_{13}$), are the most common and widespread of all sulfosalts in sulfide ore deposits (Skinner *et al.*, 1972). Mineralogical and crystallochemical aspects of natural tetrahedrite-group minerals are well known and have been studied extensively (Wuensch, 1964; Wu and Petersen, 1977; Miller and Craig, 1983; Hackbarth and Petersen, 1984; Johnson *et al.*, 1987, 1988; Makovicky, 1994; Arlt and Diamond, 1998; Fadda *et al.*, 2005; Makovicky *et al.*, 2005; Dimitrova *et al.*, 2007; Kharbish *et al.*, 2007*a*; Andreasen *et al.*, 2008; Repstock *et al.*,

2015). The simplified formula for the tetrahedrite isotopic series is $M(1)_6^{TET}M(2)_6^{TRG}[X^{TRGP}Y_3^{TET}]_4Z^{OCT}$, where $M(1)$ = Cu, Fe, Zn, Mn, Hg, Cd in tetrahedral coordination; $M(2)$ = Cu, Ag in triangular coordination; X = Sb, As, Bi, Te in trigonal coordination, X forming the top of a flat trigonal XY_3 pyramid; Y and Z = S, Se in tetrahedral (Y) or octahedral (Z) coordination (Johnson *et al.*, 1988; Moëlo *et al.*, 2008; Kharbish *et al.*, 2010). Several studies (natural and synthetic phases) have pointed out singular substitutions $((Sb \leftrightarrow As)^{TRGP}$, $(Cu^{2+} \leftrightarrow Fe, Zn)^{TET}$, $(Fe \leftrightarrow Zn)^{TET}$ and $(Ag^{+} \leftrightarrow Cu^{+})^{TRG}$), and also coupled substitutions ($(Sb \leftrightarrow As)^{TRGP} - (Ag^{+} \leftrightarrow Cu^{+})^{TRG}$) (Wu and Petersen, 1977; Miller and Craig, 1983; Sack and Loucks, 1985; Johnson *et al.*, 1986, 1987; Gemmell *et al.*, 1989; Sack and Ebel, 1993; Foit and Ulbricht, 2001; Carrillo-Rosúa *et al.*, 2008; Krismer *et al.*, 2011*a*; Vassileva *et al.*, 2013). In addition to their scientific importance, the minerals have an economic value as they are a significant source of silver (Sack and Ebel, 1993) and often contain at least trace amounts of Hg, Bi, Te, Cd, Pb and Se (Johnson *et al.*, 1986; Karup-Møller and Makovicky, 2003). Apart from the natural minerals, phase relations and thermochemistry of synthetic tetrahedrites have been studied (Skinner *et al.*, 1972; Makovicky and Skinner, 1978; Makovicky *et al.*, 2003).

Sulfosalts of Pb-Sb/As (bournonite–seligmannite, $PbCuSbS_3$ – $PbCuAsS_3$ and geocronite–jordanite $Pb_{14}Sb_6S_{23}$ – $Pb_{14}As_6S_{23}$ series) are present in variable amounts in the majority of polymetallic hydrothermal ore deposits (Ciobanu *et al.*, 2005; Buzatu *et al.*, 2015; Apopei *et al.*, 2016; Biagioni *et al.*, 2016; Vakh *et al.*, 2016). The crystal structures of bournonite and seligmannite have been solved by Takéuchi and Haga (1969) and refined by Edenharter and Nowacki (1970). Kharbish *et al.* (2010) have made important contributions to the crystal structure of bournonite. In the case of the geocronite–jordanite series, structural studies were employed by Douglass *et al.* (1954) and Birnie and Burnham (1976). Mineralogical studies regarding the compositional variability of these two solid solution series were previously reported (Wu and Birnie, 1977; Biagioni *et al.*, 2016).

Systematic vibrational studies of minerals containing isolated and interconnected pyramidal $(Sb, As)S_3$ groups were previously undertaken (Kharbish *et al.*, 2007*b*; Kharbish *et al.*, 2009; Kharbish, 2011). These pyramidal units are responsible for the Raman and infrared (IR) spectra of many sulfosalts minerals (Minceva-Sukarova *et al.*, 2003; Kharbish, 2016; Kharbish and Jeleň, 2016). In minerals that exhibit cation substitutions, major Raman band positions undergo systematic changes of spectroscopic parameters (e.g. peak shifts, changes in intensity). Therefore, Raman spectrometry reveals small changes in bond lengths and angles of crystals responding to changes in composition. Over the last few decades, numerous efforts were made to decipher the structural-spectroscopic features of different solid solution series, where Raman spectrometry can be effective as a (semi)quantitative analytical tool (Mohanan *et al.*, 1993; Kharbish *et al.*, 2007*b*; Rividi *et al.*, 2010; Buzatu *et al.*, 2013). The motivation of the present study derives from endeavours in recent years to develop efficient (semi)quantitative and qualitative Raman determinations, particularly when other methods are not available (Buzatu *et al.*, 2013; Apopei *et al.*, 2014). The aim of this study was to investigate natural tetrahedrite–tennantite, bournonite–seligmannite and geocronite–jordanite mineral series by Raman spectrometry in order to estimate the Sb/(Sb+As) content ratio. Some of the Raman spectra (of tetrahedrite–tennantite As-rich members, of bournonite–seligmannite intermediate members and of geocronite–jordanite solid solutions series), to the best of our knowledge, are presented for the first time. Also, the present paper introduces a simple and easy-to-access computer program for a fast and accurate determination of Sb/(Sb + As) contents by at least one spectroscopic parameter.

Samples and analytical methods

Samples containing tetrahedrite–tennantite, bournonite–seligmannite and geocronite–jordanite sulfosalts were collected from the Coranda-Hondol ore deposit, South Apuseni Mountains, Romania. The Coranda-Hondol deposit is an intermediate-sulfidation Au-Ag epithermal system hosted in propylitic altered andesitic rocks intruding Cretaceous and Neogene sediments (Apopei *et al.*, 2016).

Raman and electron microprobe analyses were taken at the same location in each mineral grain in order to correlate spectroscopic parameters (position, intensity and shape of the Raman peak) and chemical analyses. The chemical compositions of the investigated tetrahedrite–tennantite sulfosalts are summarized in Table 1. Those of the bournonite–seligmannite and of the geocronite–jordanite series are provided in Table 2 and Table 3, respectively.

https://doi.org/10.1180/minmag.2017.081.008 Published online by Cambridge University Press

TABLE 1. Electron microprobe analyses of tetrahedrite–tennantite minerals of the corresponding Raman spectra.

	Td_1	Td_6	Td_8	Td_{12}	Td_{15}	Td_{22}	Td_{25}	Td_{28}	Td_{36}	Td_{43}	Td_{45}	Td_{51}	Td_{59}	Td_{62}	Td_{74}	Td_{79}	Td_{83}	Td_{92}	Td_{96}	Td_{97}
wt.%																				
Cu	42.79	42.05	42.76	42.43	42.44	41.86	41.94	41.80	41.60	40.66	40.56	39.96	39.89	38.36	38.96	38.72	32.65	36.52	35.97	35.74
Ag	0.28	0.22	0.24	0.21	0.20	0.28	0.32	0.39	0.34	0.63	0.85	0.66	0.82	2.62	1.17	1.32	7.96	3.69	3.92	3.78
Pb	0.16	0.12	0.12	0.10	0.14	0.12	0.18	0.17	0.13	0.11	0.15	0.11	0.13	0.11	0.12	0.08	0.12	0.08	0.11	0.12
Fe	1.54	2.07	1.50	1.29	1.13	1.29	1.13	1.09	0.75	0.98	1.27	1.05	0.32	1.05	0.28	0.28	0.58	2.02	1.78	1.22
Zn	6.82	6.82	6.83	7.33	7.92	7.27	7.54	7.36	7.57	7.21	7.08	7.25	7.63	6.53	7.65	7.54	6.46	5.47	5.50	6.30
Mn	0.01	n.d.	0.03	n.d.	0.01	0.01	n.d.	0.02	0.01	n.d.	n.d.	n.d.	0.11	0.40	0.11	0.13	0.66	0.21	0.17	0.27
Sb	0.29	1.89	2.66	3.90	4.90	7.11	8.16	9.25	11.65	13.76	14.46	16.09	17.93	19.34	22.41	23.99	24.64	27.41	28.55	28.63
As	20.11	18.90	18.71	17.82	17.26	15.63	14.87	14.31	12.90	11.20	10.73	9.62	7.76	7.33	4.91	3.94	3.15	1.43	0.67	0.58
S	26.21	27.76	27.52	27.95	27.62	26.93	27.23	27.24	26.92	25.75	25.77	24.89	25.49	25.62	24.73	25.10	24.36	24.92	24.65	24.37
Total	98.22	99.82	100.37	101.02	101.62	100.5	101.37	101.61	101.9	100.28	100.86	99.64	100.08	101.37	100.45	101.24	100.77	101.75	101.32	101.16
Atoms per formula unit																				
Cu	10.29	9.90	10.08	9.95	9.96	10.04	10.00	9.98	10.02	10.09	10.04	10.12	10.08	9.71	10.05	9.95	8.75	9.52	9.48	9.48
Ag	0.04	0.03	0.03	0.03	0.03	0.04	0.04	0.05	0.05	0.09	0.12	0.10	0.12	0.39	0.18	0.20	1.26	0.57	0.61	0.59
Pb	0.01	0.01	0.01	0.01	0.01	0.01	0.01	0.01	0.01	0.01	0.01	0.01	0.01	0.01	0.01	0.01	0.01	0.01	0.01	0.01
Fe	0.42	0.55	0.40	0.34	0.30	0.35	0.31	0.30	0.21	0.28	0.36	0.30	0.09	0.30	0.08	0.08	0.18	0.60	0.53	0.37
Zn	1.59	1.56	1.56	1.67	1.81	1.69	1.75	1.71	1.77	1.74	1.70	1.78	1.87	1.61	1.92	1.88	1.68	1.39	1.41	1.62
Mn	-	-	-	-	-	-	-	-	-	-	-	-	-	-	-	-	-	-	-	-
Sb	0.04	0.23	0.33	0.48	0.60	0.89	1.02	1.15	1.46	1.78	1.87	2.13	2.37	2.56	3.02	3.22	3.45	3.73	3.93	3.96
As	4.10	3.77	3.74	3.54	3.44	3.18	3.01	2.90	2.63	2.36	2.25	2.07	1.66	1.57	1.07	0.86	0.72	0.32	0.15	0.13
S	12.50	12.95	12.85	12.98	12.85	12.80	12.87	12.89	12.85	12.66	12.64	12.49	12.77	12.85	12.65	12.78	12.94	12.88	12.88	12.81
∑ cat	28.99	29.00	29.00	29.00	29.00	29.00	29.01	28.99	29.00	29.01	28.99	29.01	28.97	29.00	28.99	29.00	29.01	29.02	29.00	29.00
Sb/(Sb + As)	0.01	0.06	0.08	0.12	0.15	0.22	0.25	0.28	0.36	0.43	0.45	0.51	0.59	0.62	0.74	0.79	0.83	0.92	0.96	0.97

Structural formulae calculated in atoms per formula unit (apfu) based on ∑atoms = 29; n.d. = not detected

TABLE 2. Electron microprobe analyses of bournonite–seligmannite minerals of the corresponding Raman spectra.

	Bnn_{25}	Bnn_{26}	Bnn_{40}	Bnn_{45}	Bnn_{59}	Bnn_{62}	Bnn_{72}	Bnn_{78}	Bnn_{83}	Bnn_{91}	Bnn_{93}
wt.%											
Cu	14.33	15.12	13.69	14.24	14.45	13.9	13.87	13.33	13.37	12.87	13.85
Pb	44.09	43.95	43.38	43.89	42.04	41.91	41.99	42.6	41.86	42.01	41.13
Fe	0.06	0.05	0.02	0.01	0.02	0.03	0.08	0.03	0.05	n.d.	0.03
Sb	6.53	7.12	10.56	11.63	15.77	16.00	18.59	19.93	21.57	23.2	23.65
As	12.08	12.25	9.49	8.63	6.63	6.16	4.39	3.50	2.58	1.40	1.12
Bi	0.08	0.06	0.08	0.06	0.06	0.04	0.02	0.05	0.06	0.09	0.03
Te	0.05	0.12	0.03	0.01	0.10	0.03	0.74	n.d.	n.d.	0.06	0.25
Se	0.34	n.d.	n.d.	n.d.	n.d.	n.d.	0.31	n.d.	n.d.	n.d.	n.d.
S	21.39	21.61	20.86	21.11	20.62	19.92	19.99	20.17	19.97	19.96	19.86
Total	98.95	100.26	98.09	99.57	99.69	97.98	99.99	99.62	99.47	99.59	99.93
Atoms per formula unit											
Cu	1.02	1.06	1.00	1.03	1.06	1.04	1.03	1.00	1.01	0.98	1.05
Pb	0.96	0.94	0.97	0.97	0.94	0.97	0.96	0.98	0.97	0.98	0.95
Fe	-	-	-	-	-	-	0.01	-	-	-	-
Sb	0.24	0.26	0.40	0.44	0.60	0.63	0.72	0.78	0.85	0.92	0.93
As	0.73	0.73	0.59	0.53	0.41	0.39	0.28	0.22	0.17	0.09	0.07
Bi	-	-	-	-	-	-	-	-	-	-	-
Te	-	-	-	-	-	-	0.03	-	-	-	0.01
Se	0.02	-	-	-	-	-	0.02	-	-	-	-
S	3.02	3.00	3.03	3.03	2.98	2.97	2.95	3.01	2.99	3.02	2.98
$\sum$ cat	5.99	5.99	5.99	6.00	5.99	6.00	6.00	5.99	5.99	5.99	5.99
Sb/(Sb + As)	0.25	0.26	0.40	0.45	0.59	0.62	0.72	0.78	0.83	0.91	0.93

Structural formulae calculated in atoms per formula unit (apfu) based on $\sum$atoms = 6; n.d. = not detected.

TABLE 3. Electron microprobe analyses of geocronite–jordanite minerals of the corresponding Raman spectra.

	Gcn_{24}	Gcn_{26}	Gcn_{28}	Gcn_{37}	Gcn_{40}	Gcn_{41}	Gcn_{44}	Gcn_{46}	Gcn_{47}	Gcn_{56}	Gcn_{60}	Gcn_{67}
wt.%												
Cu	0.15	0.72	0.47	0.06	0.34	0.20	0.06	0.07	n.d.	0.08	0.23	0.07
Pb	68.84	67.46	67.60	66.22	67.94	66.46	66.41	66.27	67.71	66.67	66.32	64.95
Fe	0.09	0.08	0.12	0.02	0.09	0.02	0.04	0.04	0.03	0.05	0.02	0.04
Sb	3.98	4.42	4.69	6.37	6.64	7.16	7.45	7.89	7.94	9.44	10.23	11.32
As	7.99	7.81	7.48	6.78	6.17	6.31	5.95	5.79	5.55	4.57	4.12	3.49
Bi	0.02	0.07	0.05	0.12	0.03	0.04	0.09	0.02	0.13	0.15	n.d.	0.05
Te	0.02	0.06	n.d.	0.06	0.02	0.01	n.d.	0.06	0.03	0.07	n.d.	0.03
Se	0.30	0.21	0.29	n.d.	n.d.	n.d.	n.d.	n.d.	n.d.	n.d.	0.01	n.d.
S	18.10	17.90	17.55	17.23	17.76	17.35	17.39	17.21	17.76	17.19	17.24	17.03
Total	99.49	98.72	98.25	96.86	99.00	97.54	97.39	97.35	99.15	98.22	98.18	96.98
Atoms per formula unit												
Cu	0.10	0.47	0.31	0.04	0.22	0.13	0.04	0.05	-	0.05	0.16	0.05
Pb	13.68	13.45	13.68	13.71	13.74	13.67	13.71	13.74	13.76	13.84	13.75	13.66
Fe	0.07	0.06	0.09	0.02	0.07	0.02	0.03	0.03	0.02	0.04	0.02	0.03
Sb	1.35	1.50	1.62	2.24	2.29	2.51	2.62	2.78	2.75	3.33	3.61	4.05
As	4.39	4.31	4.19	3.88	3.45	3.59	3.4	3.32	3.12	2.62	2.36	2.03
Bi	-	0.01	0.01	0.02	0.01	0.01	0.02	-	0.03	0.03	-	0.01
Te	0.01	0.02	-	0.02	0.01	-	-	0.02	0.01	0.02	-	0.01
Se	0.16	0.11	0.15	-	-	-	-	-	-	-	0.01	-
S	23.25	23.07	22.95	23.06	23.21	23.07	23.19	23.06	23.32	23.06	23.10	23.15
$\sum$ cat	43.01	43.00	43.00	42.99	43.00	43.00	43.01	43.00	43.01	42.99	43.01	42.99
Sb/(Sb + As)	0.24	0.26	0.28	0.37	0.40	0.41	0.44	0.46	0.47	0.56	0.60	0.67

Structural formulae calculated in atoms per formula unit (apfu) based on $\sum$atoms = 43; n.d. = not detected.

The identity of the sulfosalts has been firstly established based on their optical properties by using a MEIJI ML9430 microscope. The mineral phases were analysed on a Cameca SX-100 instrument, at the State Geological Institute of Dionyz Stur (Bratislava, Slovakia), equipped with energy-dispersive mode, as well as with four wavelength-dispersive spectrometers. The analytical spots were selected using back-scattered electron images. All measurements were performed on carbon-coated polished sections using an acceleration voltage of 25 kV, beam current of 15–20 nA, 4–5 μm beam diameter, 20 s count time for the peak and 7 s for the background. The following lines and standards were used (n – natural standard; s – synthetic): S*K*α (n-$CuFeS_2$), Fe*K*α (n-$CuFeS_2$), Pb*M*α (n-PbS), Cu*K*α (n-$CuFeS_2$), As*K*α, *L*α (n-FeAsS), Sb*L*β (n–Sb_2S_3), Zn*K*α (n-ZnS), Se*L*β (s-Bi_2Se_3), and pure metals for Ag*L*α, Bi*L*α, Cd*L*α and Mn*K*α. All the mineral grains and standards were analysed under the same operating conditions. The typical minimum detection limits were: 0.02 wt.% for Ag, Se, Zn, Mn, 0.03 wt.% for Fe, Cu, Sb, As, Te, Cd; 0.05 wt.% for S, 0.06 wt.% for Hg, 0.07 wt.% for Bi and 0.16 wt.% for Pb.

Samples containing tetrahedrite–tennantite, bournonite–seligmannite and geocronite–jordanite with different Sb/(Sb + As) ratios from the Coranda-Hondol ore deposit were prepared for micro-Raman spectroscopic measurements. Non-polarized micro-Raman spectra for all mineral phases were recorded in the range 1200–50 cm^{-1}, using a Horiba Jobin-Yvon – LabRam HR 800 spectrophotometer (Banská Bystrica, Slovakia). The 632.8 nm excitation line of a He-Ne laser (17 mW) was focused with a 100×/0.80 Olympus objective on the sample surface. The experimental parameters were 40 s exposure time, 3–4 exposures, 600 lines/mm grating. The laser power was controlled by means of a series of density filters in order to avoid heating effects. The grating turret accuracy was calibrated between zero-order line (180° reflection) and laser line at 0 cm^{-1}. Accuracy was verified via the ν_1 peak of silicon which was always lying within three detector pixels around the theoretical value (520.7 cm^{-1}). The system resolution was 2 cm^{-1}, and the wavenumber accuracy was ± 1 cm^{-1}. The instrument includes a confocal mode system. A 532 nm laser were used, but the Raman spectra obtained in the present study using excitation wavelengths of 632.8 nm were of higher quality, in terms of signal-to-noise ratio and photochemical degradation. Baseline corrections and peak centres of single bands were determined by fits of combined Gaussian/Lorentzian amplitude functions using *PeakFit 4.12* software (Jandel Scientific).

Results

Chemistry of the samples

The chemical formulae of the tetrahedrite–tennantite, bournonite–seligmannite and geocronite–jordanite series were calculated on the basis of 29, 6 and 43 atoms per formula unit (apfu), respectively. One of the most common substitutions that may occur in the tetrahedrite–tennantite, bournonite–seligmannite and geocronite–jordanite series is between Sb and As, defining the end-members of each series, as follows: tetrahedrite $(Cu,Ag)_{10}(Fe,Zn)_2Sb_4S_{13}$ – tennantite $(Cu,Ag)_{10}(Fe,Zn)_2As_4S_{13}$), bournonite ($PbCuSbS_3$) – seligmannite ($PbCuAsS_3$) and geocronite ($Pb_{14}Sb_6S_{23}$) – jordanite ($Pb_{14}As_6S_{23}$). The chemical composition for the sulfosalts used in this study will be expressed as Td_x ($tetrahedrite_x$), Bnn_x ($bournonite_x$) and Gcn_x ($geocronite_x$), where $x = Sb/(Sb + As) \times 100$ (apfu). Electron microprobe data for the identified sulfosalts reveal the existence of extensive solid solution series (Td_1 to Td_{97}, Bnn_{25} to Bnn_{93} and Gcn_{24} to Gcn_{67}, apfu). A strong correlation between Sb and As ($r = 0.99$) for each series confirms the absence of other substitutions in the X^{3+} site of the trigonal pyramidal group unit (i.e. XS_3).

Micro-Raman spectra and band assignments

Raman bands appear between 400 and 50 cm^{-1}. No additional bands were observed in the region 1200–400 cm^{-1}. The region between 400 and 200 cm^{-1} is characteristic of normal vibrational modes of sulfides (Wang *et al.*, 1994), while Raman bands below 200 cm^{-1} arise from lattice vibrations (Kharbish and Jeleň, 2016). From 400–200 cm^{-1}, Raman spectra of tetrahedrite–tennantite series (Td_1–Td_{97}) show characteristic bands (Fig. 1) similar to those reported by Kharbish *et al.* (2007*b*) for Td_0 and between Td_{55}–Td_{98} members. In the tennantite end-member (Td_1), the very strong band assigned to symmetric As–S stretching (ν_{1tn}) occurs at 383 cm^{-1}. The antisymmetric stretching mode (ν_{3tn}) is present as a shoulder at 372 cm^{-1}. Weak and broad bands at 342 and 312 cm^{-1} are assigned to ν_{2tn} symmetric bending and ν_{4tn} antisymmetric bending modes of the AsS_3 group, respectively. For the tetrahedrite

https://doi.org/10.1180/minmag.2017.081.008 Published online by Cambridge University Press

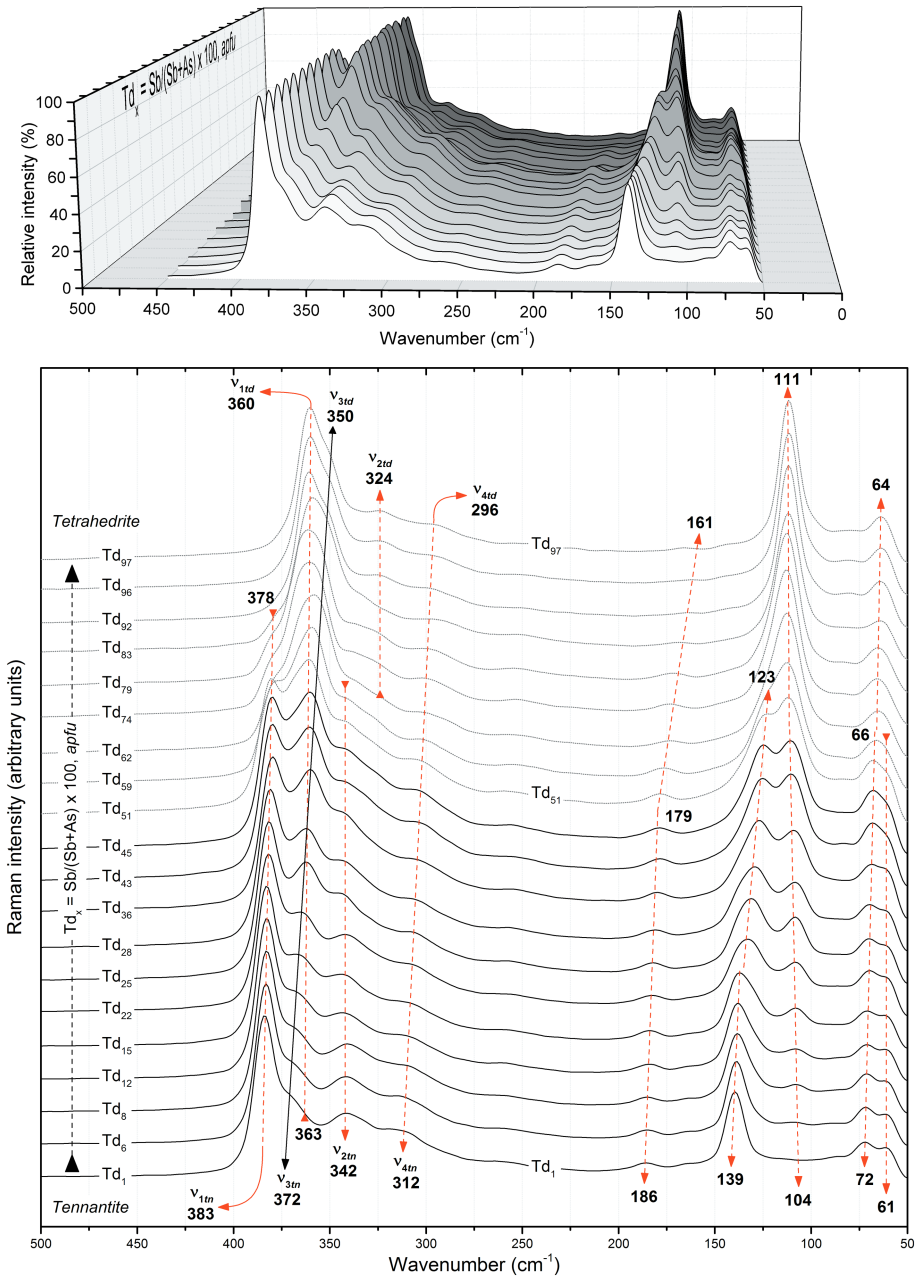

FIG. 1. Representative Raman spectra of tetrahedrite–tennantite solid solution series. Spectra are vertically offset for clarity. Chemical analyses for each member of the series are shown in Table 1.

end-member (Td_{97}), the strong band at 360 cm^{-1} is assigned to Sb–S stretching (ν_{1td}). The medium intensity shoulder at 350 cm^{-1} is assigned to antisymmetric stretching (ν_{3td}), while the ν_{2td} symmetric bending and ν_{4td} antisymmetric bending modes appear as weak and broad peaks at 324 and 296 cm^{-1}, respectively (Fig. 1). In the Raman spectra of intermediate members of

https://doi.org/10.1180/minmag.2017.081.008 Published online by Cambridge University Press

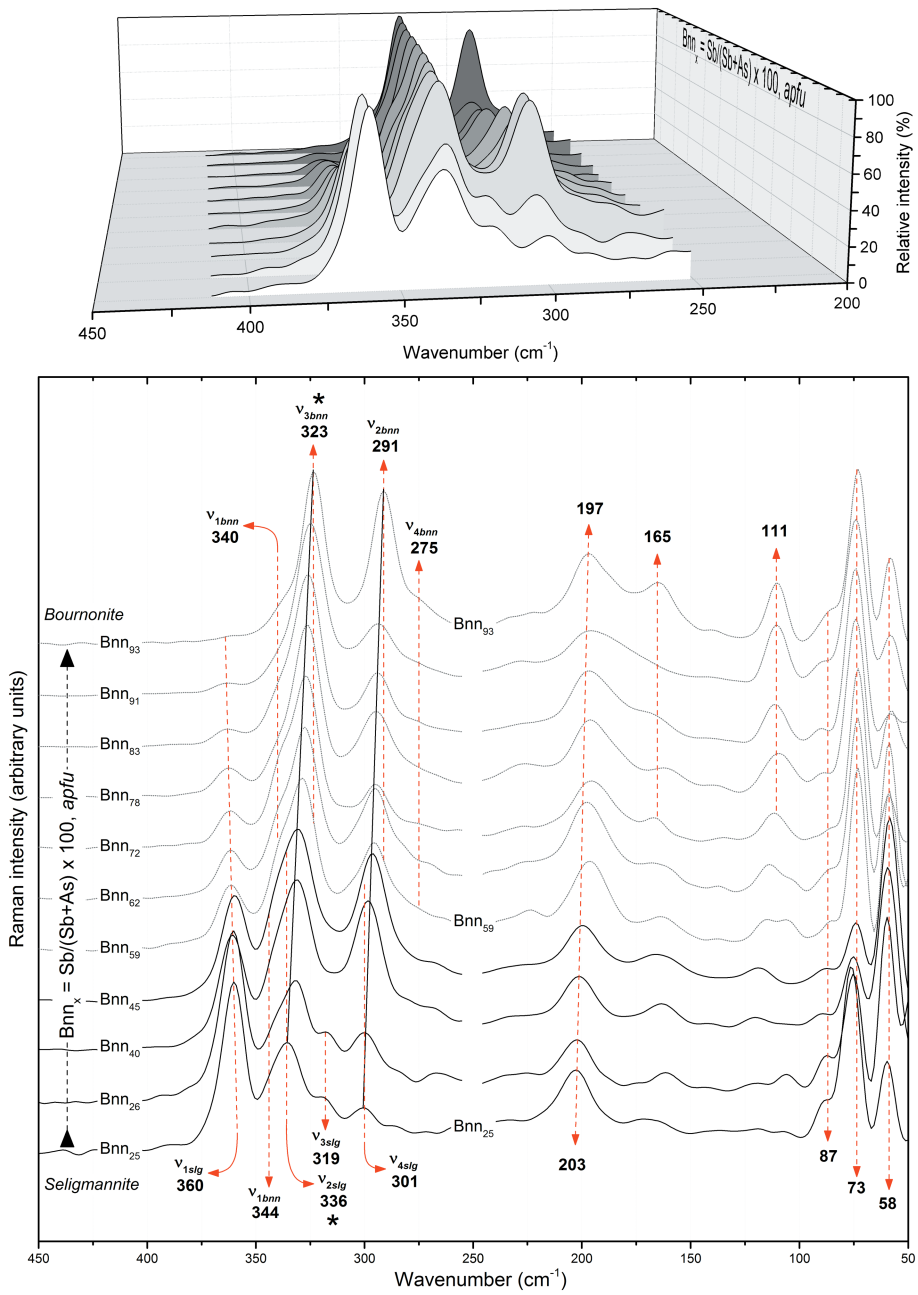

FIG. 2. Representative Raman spectra of bournonite–seligmannite solid solution series. Spectra are vertically offset for clarity. Chemical analyses for each member of the series are shown in Table 2.

tetrahedrite–tennantite series vibrations of As–S and of Sb–S are seen. Lattice vibrations are found at 186, 139, 104, 72 and 61 cm^{-1} for Td_1 and at 161, 111 and 64 cm^{-1} for Td_{96}.

Raman spectra of the bournonite–seligmannite series (Bnn_{25}–Bnn_{93}) are shown in Fig. 2. The Raman spectrum of Bnn_{35} (seligmannite) shows a very strong band at 360 cm^{-1} assigned to ν_{1slg}

https://doi.org/10.1180/minmag.2017.081.008 Published online by Cambridge University Press

symmetric stretching. The ν_{3slg} antisymmetric stretching mode (at 319 cm^{-1}) is present as a shoulder of the ν_{2slg} mode (at 336 cm^{-1}), while the ν_{4slg} antisymmetric bending mode is present as a weak band at 301 cm^{-1}. For the bournonite spectrum (Bnn_{93}), two dominant bands appear at 323 and 291 cm^{-1}, assigned to ν_{3bnn} and ν_{2bnn}, respectively. The symmetric stretching mode (ν_{1bnn}) appears as a shoulder at 340 cm^{-1}. The weak shoulder band at 275 cm^{-1} is assigned to the antisymmetric S–Sb–S bending mode (ν_{4bnn}). Both vibrations of As–S and Sb–S symmetric stretching arise in the Raman spectra of intermediate members of bournonite–seligmannite series. Lattice vibrations are found at 203, 87, 73 and 58 cm^{-1} for Bnn_{35} and at 197, 165, 111, 87, 73 and 58 cm^{-1} for Bnn_{93}. Very weak additional shoulder bands occur in Bnn–Slg series in the region below 200 cm^{-1}. Raman bands for the Sb and As-rich members of the series are in good agreement with literature data for bournonite (Bnn_{100}; Kharbish *et al.*, 2009) and seligmannite (Bnn_5; Kharbish, 2016). For different compositions of the solid solution $PbCu(Sb_xAs_{1-x})S_3$ no Raman data have been published so far.

The Raman spectra for the geocronite–jordanite series (Gcn_{24}–Gcn_{67}) is shown in Fig. 3. In the region between 400 and 200 cm^{-1}, a group of broad weak- to medium-intensity bands and shoulders are readily observed. The symmetric stretching mode (ν_{1jor}) appears at 377 cm^{-1} for Gcn_{24} and at 373 cm^{-1} (ν_{1gcn}) in the case of Gcn_{67}. The ν_2 symmetric bending mode is attributed to the weak and broad band at 300 cm^{-1}. The other two normal modes (i.e. ν_2 and ν_3) arise as shoulders or very broad peaks between 400 and 250 cm^{-1}. In the lower wavenumber region (below 200 cm^{-1}), two prominent strong bands arise at 72 and 59 cm^{-1}. Compared to the Raman spectra obtained on the Td–Tn and Bnn–Slg series, the Gcn–Jor Raman spectra shows several broad and weak bands in the range below 200 cm^{-1}, some of which cannot be seen very clearly by visual inspection alone. Raman bands which arise in the lower wavenumber region (200–50 cm^{-1}) can be assigned to lattice vibrations. Raman data for the geocronite–jordanite series, to the best of our knowledge, have not been published so far.

Discussion

According to Nakamoto (1997), the isolated ideal trigonal symmetry (C_{3v} point group) of the XY_3 pyramid shows only four normal Raman- and IR-active modes of vibration (i.e. $2A_1 + 2E$). Nakamoto (1997) also mentions that two stretching vibrations, ν_1 (A_1, symmetric) and ν_3 (E, antisymmetric) are close in energy or overlap. The other two bending vibrations, ν_2 (A_1, symmetric) and ν_4 (E, antisymmetric) show the same behaviour; in terms of band energies, the band assignments are based on the sequence $\nu_1 > \nu_3 > \nu_2 > \nu_4$ (Nakamoto, 1997). According to Kharbish *et al.* (2007*b*), the spectroscopic features of the tetrahedrite–tennantite solid solution series are caused by vibrations of the isolated pyramidal four atom groups $(Sb,As)S_3$ of ideal trigonal symmetry. Despite the presence of singular and coupled substitutions that may occur in fahlore minerals (e.g. Td_{83} with 7.96 wt.% Ag), changes of parameters (i.e. band position, intensity or shape) are caused only by the Sb/(Sb + As) ratio.

Raman spectra of the studied fahlore samples (shown in Fig. 1) show similar trends of the ν_1, ν_2, ν_3 and ν_4 vibrations as pointed out by Kharbish *et al.* (2007*b*) for the Td_0 and Td_{55}–Td_{98} range of compositions determined by energy-dispersive analysis. They clearly show that band shape, position and intensity of the normal vibrations (in the range 450–200 cm^{-1}) depend on Sb/(Sb + As) ratios. The most notable evolution of band positions in relation to the Sb/As content is shown by the ν_4 vibration (Fig. 1). The three other modes of normal vibrations (ν_1, ν_2 and ν_3) show a slight evolution (i.e. in a narrow range). The extended range (between 200–50 cm^{-1}) compared to the existing literature data of tetrahedrite–tennantite series (450–250 cm^{-1}; Kharbish *et al.*, 2007*b*) revealed new patterns of lines in relation to increasing Sb/(Sb + As) ratio.

By inspecting the low-wavenumber region (below 200 cm^{-1}) of the fahlore Raman spectra obtained between Td_1–Td_{97} chemical range, a clear evolution of bands can be observed, either in terms of position and intensity or by shape of bands (Fig. 4). One of the most visible evolutions of this kind appears in the case of the 139 cm^{-1} strong band (for Td_1) which evolves towards lower wavenumbers (123 cm^{-1} for Td_{51}, and finally is incorporated by the most prominent band at 111 cm^{-1} for Td_{97}). Another obvious evolution of the Raman spectra of tetrahedrite–tennantite series can be observed in the case of the very weak band at 104 cm^{-1} (Td_1). This band shows two-mode behaviour by increasing in intensity and also by moving towards higher wavenumbers (111 cm^{-1}, for Td_{97}) in relation to the Sb/(Sb + As) ratio. Other evolutions of the Raman spectra worth mentioning are those of the very weak and broad band position,

https://doi.org/10.1180/minmag.2017.081.008 Published online by Cambridge University Press

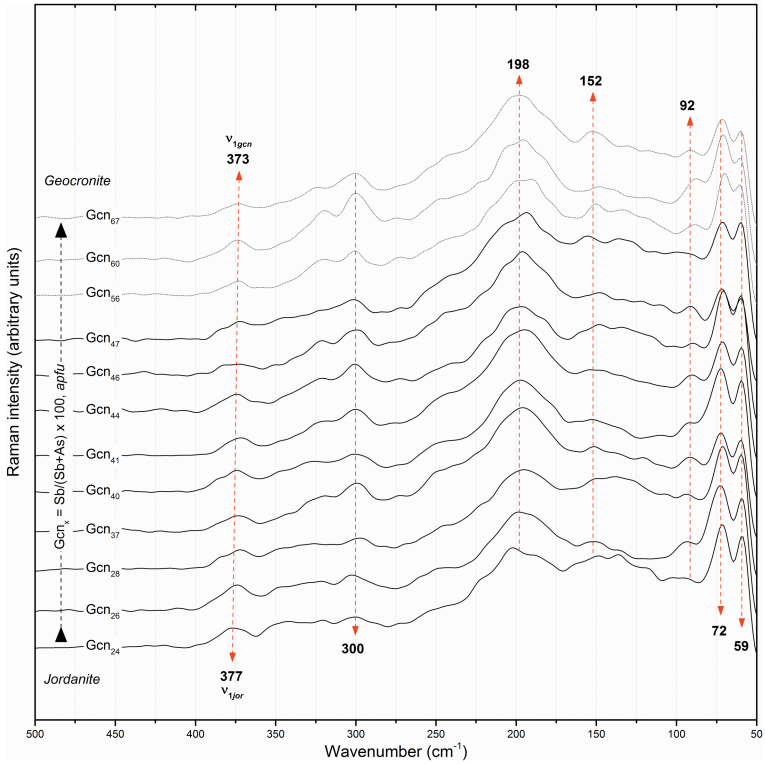

FIG. 3. Representative Raman spectra of the geocronite–jordanite solid solution series. Spectra are vertically offset for clarity. Chemical analyses for each member of the series are shown in Table 3.

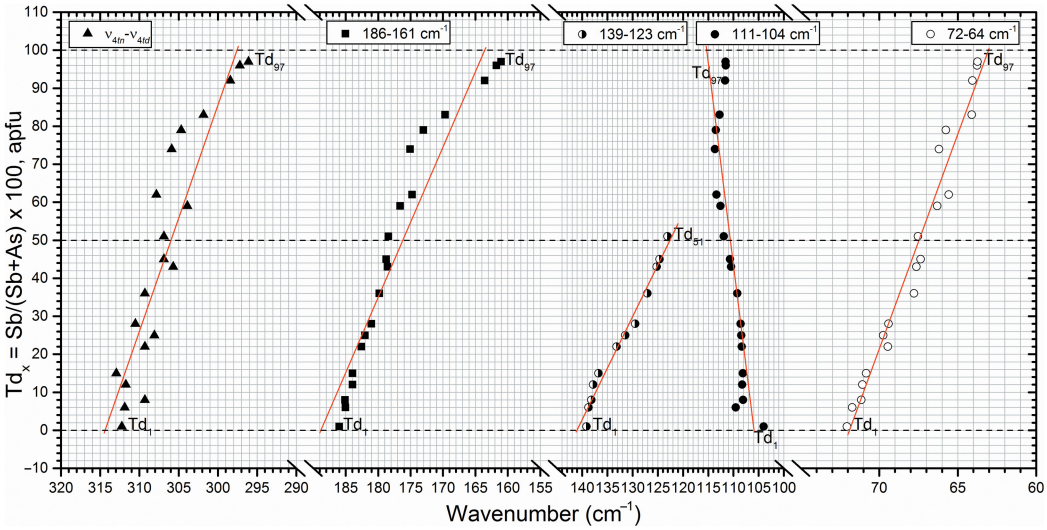

FIG. 4. Correlation between Raman bands position (cm^{-1}) and the Sb/(Sb + As) content ratio of the tetrahedrite–tennantite solid solution series.

https://doi.org/10.1180/minmag.2017.081.008 Published online by Cambridge University Press

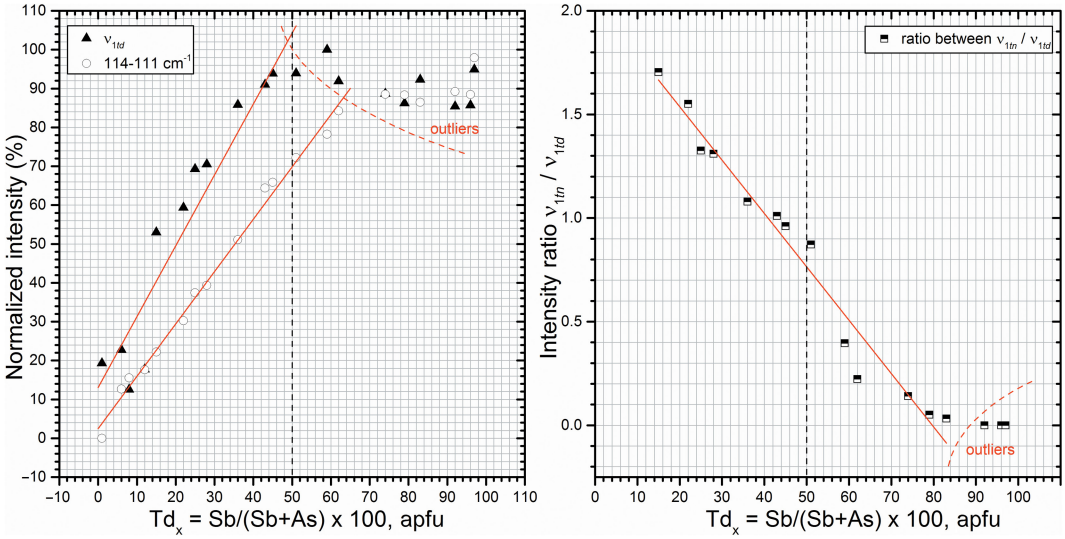

FIG. 5. Correlation between relative Raman bands intensities (%) and the Sb/(Sb + As) content ratio of the tetrahedrite–tennantite solid solution series.

centred at 186 cm^{-1}, of the tennantite end-member (Td_1) which evolves consistently to lower wavenumbers (161 cm^{-1}) with increase of the Sb/(Sb + As) ratio. Furthermore, for the composition range Td_{92}–Td_{97}, these bands decrease in intensity. The doublets at 72 and 61 cm^{-1} (Td_1) also show a slight change regarding band shape and the position in the form of an increase in the Sb/(Sb + As) ratio. In Sb-rich members, these bands are incorporated into a single broad band centred at 64 cm^{-1} (Td_{97}).

The recommended method of estimating the Sb/(Sb + As) ratio in fahlore samples involves using the following linear equations of the first-order polynomial fit obtained in Fig. 4:

$$\nu_{4td} - \nu_{4tn}\left(312 - 296\,cm^{-1}\right), \quad y = 1869.5729 - (5.9468 \times x) \tag{1}$$

$$186–161\,cm^{-1}\ mode, \quad y = 747.1607 - (3.9567 \times x) \tag{2}$$

$$139–123\,cm^{-1}\ mode, \quad y = 382.3759 - (2.7112 \times x) \tag{3}$$

$$111–104\,cm^{-1}\ mode, \quad y = -1128.9249 + (10.6578 \times x) \tag{4}$$

$$72–64\,cm^{-1}\ mode, \quad y = 811.9814 - (11.2935 \times x) \tag{5}$$

where y is Sb/(Sb + As) × 100 (apfu), and x is the wavenumber values of the Raman bands.

In addition, a strong correlation was found between the relative intensity of the symmetric stretching mode ν_{1td} (centred at 363 cm^{-1}) and the Sb/(Sb + As) ratio. The 363 cm^{-1} Raman band shows a linear decrease in intensity following Sb-to-As substitution (Fig. 5). We also noticed that the intensity ratio between ν_{1tn} and ν_{1td} increases with As concentration. By plotting the relative intensity *vs.* the Sb/(Sb + As) ratio (Fig. 5), the following equations of the first-order polynomial fit were obtained.

$$\nu_{1td}\left(363\,cm^{-1}\right),\ x = \frac{(y - 13.0507)}{1.8242} \tag{6}$$

$$114–111\,cm^{-1}\ mode,\ x = \frac{(y - 2.4886)}{1.3467} \tag{7}$$

$$\text{ratio between } \nu_{1tn}/\nu_{1td},\ x = \frac{(y - 2.0520)}{-0.0258} \tag{8}$$

where x is Sb/(Sb + As) × 100 (apfu), and y is the relative band intensities.

Raman spectra of tetrahedrite with elevated Ag content (up to 21.4 wt.% Ag) were reported for the first time by Buzatu *et al.* (2017). The effect on the Raman bands of Ag is noticeable in the case of fundamental modes (ν_1, ν_2, ν_3 and ν_4). These vibrations are observable at lower wavenumbers than the typical tetrahedrite values, with differences of 12–17 cm^{-1} (Buzatu *et al.*, 2017). In the case of lattice vibrations, the elevated Ag content does not

https://doi.org/10.1180/minmag.2017.081.008 Published online by Cambridge University Press

influence so much the shifting of Raman bands (2–3 cm^{-1}).

It is well known that Ag preferentially substitutes Cu at the *M*(2) site, located in the cavity of the tetrahedral framework (Johnson *et al.*, 1988). At the same time, Johnson *et al.* (1988) note that the length of the so-called spinner blades (i.e. six (Cu, Ag)S_3 groups) of the tetrahedrite framework cavity increases as a function of the Ag content. This expansion affects the rotation of the tetrahedral framework (i.e. $M(1)Y_4$ tetrahedra), leading to an increase of the bonds length from the XY_3 groups (Johnson *et al.*, 1988). As a result, the increase of the Sb–S bond length from XY_3 pyramids causes the fundamental modes to be shifted to lower wavenumbers. Similar Raman behaviour for tetrahedrite with elevated Ag contents was also reported by Krismer *et al.* (2011*b*), but with smaller differences between peak values, as the authors presented Raman data for only one sample with 10.5 wt.% Ag. In Fig. 1, the Raman spectrum of Td_{83} with Ag content of 7.96 wt.%, presents the same behaviour, having the main vibrational modes shifted to lower wavenumbers (4 cm^{-1}), but with no influence on lattice vibrations.

Pattrick and Hall (1983) pointed out that the increase of the cell size as a function of Ag content is not a constant function, being lowest for low Ag tetrahedrites and increasing at a faster rate for tetrahedrites with Ag content higher than 3 apfu. Regarding the lattice vibrations noticed by Buzatu *et al.* (2017) in Ag-rich tetrahedrites, the evolution of the spectroscopic lines (in terms of intensity or of shape of bands) is similar with what we observed in the case of tetrahedrite with no Ag content (Fig. 1 and 4). Moreover, considering the fact that the fahlore samples analysed in the present study are of Zn-type and those from Buzatu *et al.* (2017) are of Fe-type, it can be postulated that the evolution of the lattice vibrations and the correlations obtained in Fig. 4 are caused mainly by the Sb–As substitution within the structure. Taking into account the above, it can be deduced that the shift to lower wavenumbers based on the increase of Ag content is not a linear function and has a bigger impact on tetrahedrites with an Ag content higher than 10 wt.%. Also, compared to the fundamental modes, lattice vibrations are less affected by increasing of Ag content.

In the bournonite–seligmannite series, (Sb,As)S_3 pyramids are different from those in the tetrahedrite–tennantite series by the symmetry of the four atom pyramidal groups, which is reduced from C_{3v} to C_s. Moreover, two different *X* sites of the XS_3 pyramidal groups are present in the structure of the bournonite–seligmannite series. Therefore, different Sb and As atoms, Sb(1), Sb(2), As(1) and As(2) form isolated and slightly distorted (non-trigonal) pyramidal units. The latest refinement of the bournonite structure (Kharbish *et al.*, 2010), contrary to the structure data of Edenharter and Nowacki (1970), shows that the Sb–S distances of both crystallographic *X* sites, Sb(1) and Sb(2), are almost equal. Consequently, the splitting or increasing of the normal modes is caused only by lowered symmetry which controls the molecular vibrations in the crystals (Nakamoto, 1997).

For the bournonite–seligmannite series, with the chemical composition ranging between Bnn_{25} and Bnn_{93}, Raman spectra show an evolution of the bands depending on the Sb/(Sb + As) ratio (Fig. 2). Most notable is in the case of the very strong Raman band centred at 360 cm^{-1} which decreases in intensity as the Sb/(Sb + As) ratio increases. Kharbish *et al.* (2009) pointed out that the Raman spectrum of the bournonite end-member (Bnn_{100}) is characterized by a strong variation of band intensities relative to the laser polarization direction. According to the above and considering the Raman spectra of Bnn_{25}–Bnn_{93} obtained in the present study, the band centred at 336 cm^{-1} (ν_{2slg}) which is shifted to lower wavenumber (323 cm^{-1}, ν_{3bnn}) with increasing Sb/(Sb + As) ratio can be correlated with the Sb/As content, rather than being a cause of the laser polarization direction. Although these lines incorporate (as shoulders) another vibration, the maxima of this band can be used for the determination of Sb/(Sb + As) content. Therefore, peak fitting reveals a two-mode behaviour of the 336 cm^{-1} band by increasing in intensity and also by moving towards lower wavenumbers. Raman bands which may be related to the laser polarization direction are those from 291–301 cm^{-1} and the strongest peaks from 73 and 58 cm^{-1}. No other correlation between line parameters (band position, intensity or shape) was found in the bournonite–seligmannite Raman spectra. To estimate the Sb/(Sb + As) ratio by the Raman band position or by relative intensities of the ν_{1slg} symmetric stretching mode, the following linear equation of the first-order polynomial fit was used (Fig. 6 and 7):

$$\nu_{2slg} - \nu_{3bnn}, y = 2684.6108 - (7.9914 \times x) \quad (9)$$

where *y* is Sb/(Sb + As) × 100 (apfu), and *x* is the

https://doi.org/10.1180/minmag.2017.081.008 Published online by Cambridge University Press

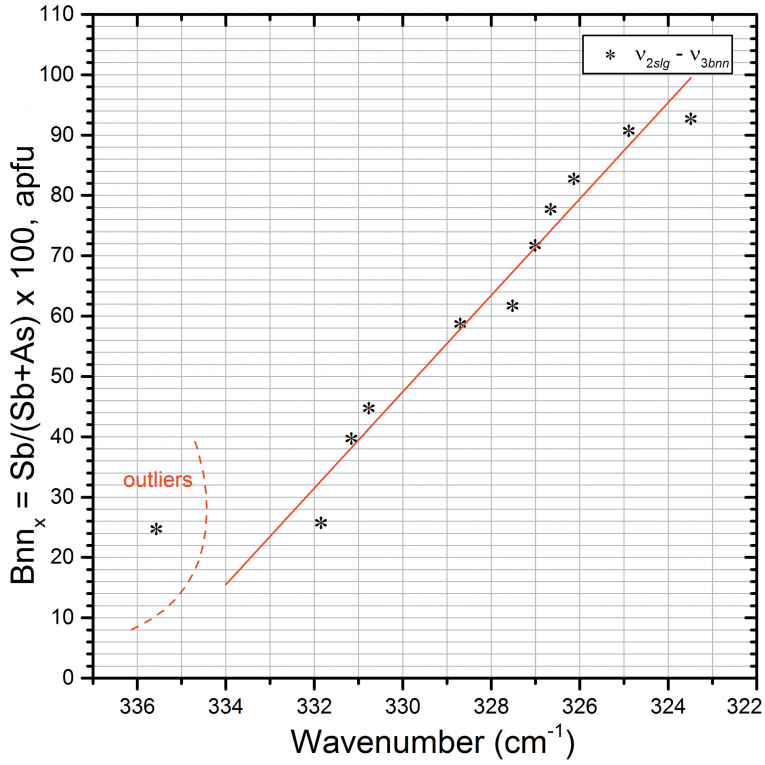

FIG. 6. Correlation between Raman bands position (cm^{-1}) and the Sb/(Sb + As) content ratio of the bournonite–seligmannite solid solution series.

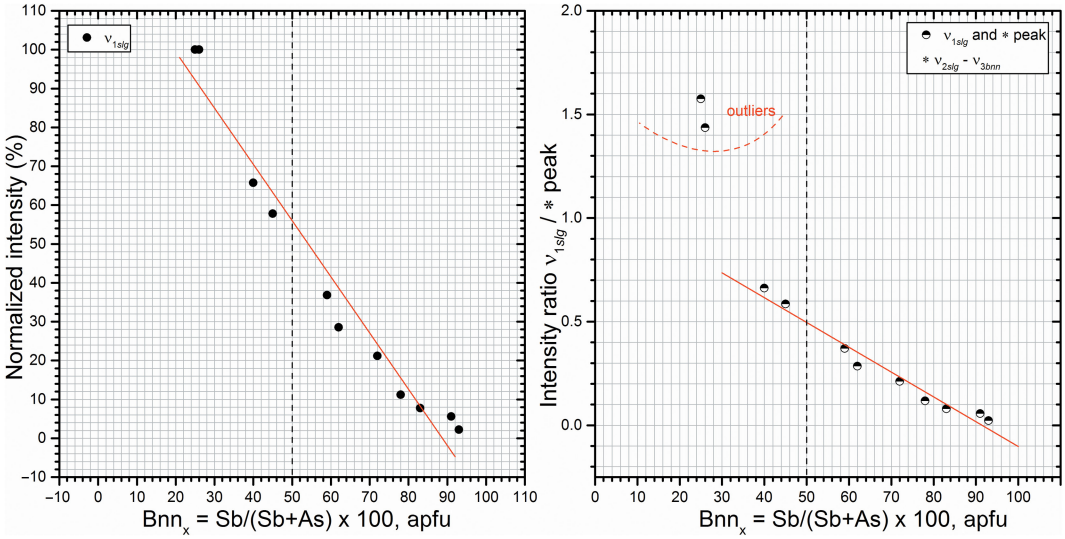

FIG. 7. Correlation between relative Raman bands intensities (%) and the Sb/(Sb + As) content ratio of the bournonite–seligmannite solid solution series.

https://doi.org/10.1180/minmag.2017.081.008 Published online by Cambridge University Press

wavenumber values of the Raman bands.

$$\nu_{1slg},\ x = \frac{(y - 128.3422)}{-1.4466} \quad (10)$$

$$\nu_{1slg}/\nu_{2slg} - \nu_{3bnn},\ x = \frac{(y - 1.09471)}{-0.0120} \quad (11)$$

Here, x is Sb/(Sb + As) × 100 (apfu), and y is the relative band intensities.

The crystal structure of the geocronite–jordanite series shows a more complex site occupancy than that of the tetrahedrite–tennantite and bournonite–seligmannite sulfosalts. According to Biagioni *et al.* (2016), in the geocronite–jordanite series, the semi-metallic XS$_3$ pyramids have four different X sites: Sb(4), As(6), As(11) and the split position Pb(2a)/Sb(2b). The same authors suggest that the Sb-to-As substitution takes place preferentially at the Sb(4) and As(6) sites, whereas only members having Sb contents higher than 4 apfu should host Sb at the As(11) site. Taking into consideration the X–S (X = Sb, As) interatomic distance of geocronite–jordanite (2.407–2.253 Å; Biagioni *et al.*, 2016), and the observations made by Kharbish and Jeleň (2016) for minerals containing XS$_3$ pyramids, the normal vibrations of geocronite–jordanite are expected at higher wavenumbers due to the shortest X–S distance. In contrast to the previously discussed sulfosalt series (Td–Tn and Bnn–Slg), Raman spectra of geocronite–jordanite (Gcn$_{24}$–Gcn$_{67}$) do not show any evolution of the Raman bands depending on the Sb/(Sb + As) ratio. The mixed Sb-As sites of geocronite–jordanite may be the reason for these missing correlations.

jSulfoQuant – a computer program for Sb/(Sb + As) content ratio determination by means of Raman spectrometry

In order to make the identification process easier, a computer program (*jSulfoQuant* – http://jsulfoquant.sf.net) was created for the determination of the Sb/(Sb + As) ratio of the tetrahedrite–tennantite and bournonite–seligmannite solid solutions. This program can be downloaded from the above-mentioned website. The *jSulfoQuant* software is written entirely in Java language, which uses the principles of the Java Virtual Machine (JVM). Java is a simple, object-oriented, distributed and interpreted programming language, which offers high security, portability (OS independent) and performance, as well as support for multithreading.

The *jSulfoQuant* application consists of a well-organized and optimized layout for the visual inspection of the specific Raman spectrum. The application can open any file with the extension .txt, .rruff, .csv, .asc or .dat and a two column data format, where the values in the first column are assumed to be the wavenumber (X axis), and those in the second column designate intensity (Y axis). The *jSulfoQuant* program supports the following file format delimiters: (1) tab delimiter; (2) space; (3) comma; (4) semicolon, and it can even ignore rows which start with ##comments. These delimiters increase the possibility of opening spectra which are formatted in different ways (this occurs when different types of spectroscopic instruments and/or standardization are used). For example, the files of the RRUFF project (Lafuente *et al.*, 2015) contain a two number sign (i.e. two hashtag symbols: ##) for each line that includes name, locality, id and chemistry of the sample.

For a fast and accurate determination of the Sb/(Sb + As) ratio of tetrahedrite–tennantite and bournonite–seligmannite solid solution series using *jSulfoQuant* software, all of the correlations discussed previously were taken into account. The procedure of Sb/(Sb + As) ratio determination was developed using a three-step approach. First, a Raman spectrum is required to be loaded into the chart panel by using 'New' or 'Open Spectrum' function (Fig. 8*a*). Second, the user needs to choose between tetrahedrite–tennantite and bournonite–seligmannite solid solution series and also for at least one spectroscopic parameter (Fig. 8*b*). Finally, the calculation is performed by pressing the 'Calculate' button. The obtained value is expressed as Sb/(Sb + As) × 100 (apfu) and plotted into the correspondent interactive correlation chart (Fig. 8*c*). The software was successfully tested on Zn- and Fe-tetrahedrites. Considering the fact that the software is based on the correlations of Figs 4 to 7, which were obtained on natural tetrahedrites with an Ag content up to 7.96 wt.%, it is recommended to be used with caution in the case of Ag-bearing tetrahedrites (especially in the case of correlations that involve the fundamental modes). Apart from this function to determine the Sb/(Sb + As) ratio, the *jSulfoQuant* application is designed to offer several tools necessary for the manipulation of the Raman spectrum. The Raman spectra opened from the local computer can be visually explored in different ways, thus providing a series of functionalities. They include zooming and rescaling of the Raman spectrum, and dragging, peaking, printing and showing of the coordinates as the mouse moves over the spectrum. Future improvements of this software will concentrate on extending the mineral series.

https://doi.org/10.1180/minmag.2017.081.008 Published online by Cambridge University Press

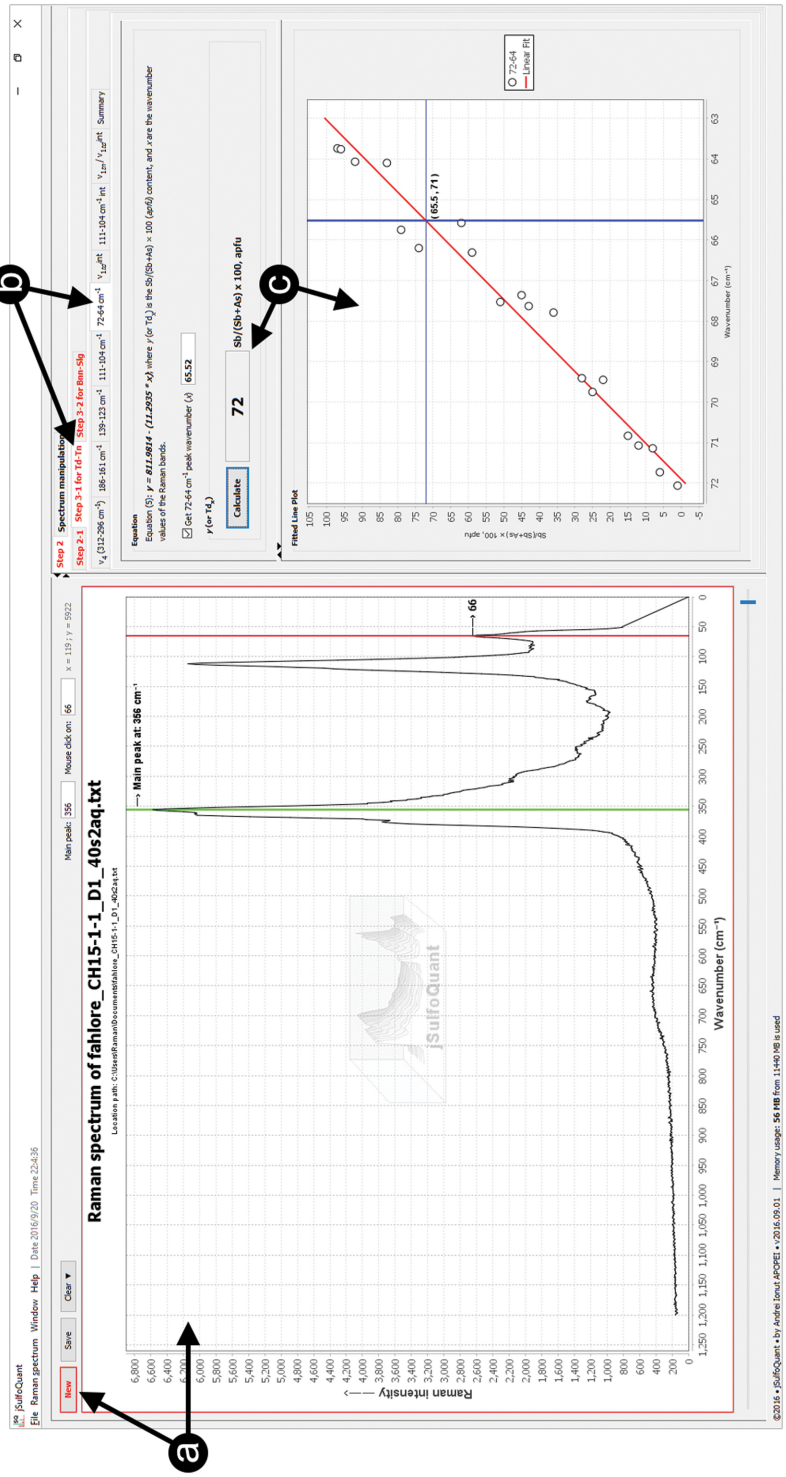

FIG. 8. Layout of the main window of the *jSulfoQuant* application with a Raman spectrum opened and Sb/(Sb + As) content ratio calculation performed. The procedure of Sb/(Sb + As) content ratio determination was developed using a three-step approach: (*a*) Raman spectrum is required to be loaded into the chart panel by using 'New' or 'Open Spectrum' functions. The user needs to choose between tetrahedrite–tennantite and bournonite–seligmannite solid solution series and also for at least one spectroscopic parameter. Finally, the calculation is performed by pressing the 'Calculate' button. The obtained value is expressed as Sb/(Sb + As) × 100 (apfu) and plotted in the interactive correlation chart.

https://doi.org/10.1180/minmag.2017.081.008 Published online by Cambridge University Press

Conclusions

This study reveals a close link between the Raman spectra of sulfosalts containing XS_3 pyramids (X = Sb, As) and their chemical composition. Also, this study fills the gaps regarding the Raman characteristics of fahlore minerals for compositional range Td_1–Td_{54}. New Raman spectra of bournonite–seligmannite and geocronite–jordanite intermediate solid solution series (Bnn_{25}–Bnn_{93} and Gcn_{24}–Gcn_{67}) are presented for the first time. The results obtained in the present study provide the Sb/(Sb + As) ratio by determining the position or relative intensity of at least one Raman band in the spectrum of the tetrahedrite–tennantite and bournonite–seligmannite solid solution series. Accordingly, eight linear equations for tetrahedrite–tennantite and three for bournonite–seligmannite were obtained. Due to the mixed Sb-As sites of the geocronite–jordanite members of the series, no correlation exists between spectroscopic parameters and Sb/(Sb + As) ratio. In order to ease the identification process, a computer program was developed for a fast and accurate determination of the Sb/(Sb + As) ratio. With lower excitation efficiency and fluorescence, the 632.8 nm laser provides the best performance and is suitable for the tetrahedrite–tennantite, bournonite–seligmannite and geocronite–jordanite solid solution series. The present study has revealed the usefulness of Raman spectroscopy for (semi) quantitative measurements of tetrahedrite–tennantite and bournonite–seligmannite mineral series.

Acknowledgements

The authors gratefully acknowledge the staff of S.C. Deva Gold S.A. for providing access to the Coranda-Hondol open pit and for their on-site support. Thanks are also due to the staff of the laboratory of electron microanalysis of the State Geological Institute of Dionýz Štúr, Bratislava, Slovakia; Konečný Patrik, Ivan Holický and Viera Kollárová for EPMA analyses. Thanks are also due to David Alderton for his valuable comments that helped to improve the initial version of the manuscript. This work was supported by the "Alexandru Ioan Cuza" University of Iasi, within "*UAIC Grants for young researchers*" (project GI - 2015 - 08).

References

Andreasen, J.W., Makovicky, E., Lebech, B. and Møller, S.K. (2008) The role of iron in tetrahedrite and tennantite determined by Rietveld refinement of neutron powder diffraction data. *Physics and Chemistry of Minerals*, **35**, 447–454.

Apopei, A.I., Buzgar, N., Damian, G. and Buzatu, A. (2014) The Raman study of weathering minerals from the Coranda-Hondol open pit (Certej gold-silver deposit) and their photochemical degradation products under laser irradiation. *Canadian Mineralogist*, **52**, 1027–1038.

Apopei, A.I., Damian, G., Buzgar, N. and Buzatu, A. (2016) Mineralogy and geochemistry of Pb–Sb/As-sulfosalts from Coranda-Hondol ore deposit (Romania) – conditions of telluride deposition. *Ore Geology Reviews*, **72**, 857–873.

Arlt, T. and Diamond, L.W. (1998) Composition of tetrahedrite-tennantite and 'schwazite' in the Schwaz silver mines, north Tyrol, Austria. *Mineralogical Magazine*, **62**, 801–820.

Biagioni, C., Dini, A., Orlandi, P., Moelo, Y., Pasero, M. and Zaccarini, F. (2016) Lead-antimony sulfosalts from Tuscany (Italy). XX. Members of the jordanite-geocronite series from the Pollone mine, Valdicastello Carducci: occurrence and crystal structures. *Minerals*, **6**, 15; https://doi.org/10.3390/min6010015

Birnie, R. and Burnham, C.W. (1976) The crystal structure and extent of solid solution of geocronite. *American Mineralogist*, **61**, 963–970.

Buzatu, A., Buzgar, N., Damian, G., Vasilache, V. and Apopei, A.I. (2013) The determination of the Fe content in natural sphalerites by means of Raman spectroscopy. *Vibrational Spectroscopy*, **68**, 220–224.

Buzatu, A., Damian, G., Dill, H.G., Buzgar, N. and Apopei, A.I. (2015) Mineralogy and geochemistry of sulfosalts from Baia Sprie ore deposit (Romania) – new bismuth minerals occurrence. *Ore Geology Reviews*, **65**, 132–147.

Buzatu, A., Damian, G., Buzgar, N., Andráš, P., Apopei, A.I., Maftei, A.E. and Milovska, S. (2017) Structural key features of bismuth and Sb-As sulfosalts from hydrothermal deposits – micro-Raman spectrometry. *Vibrational Spectroscopy*, **89**, 49–56.

Carrillo-Rosúa, J., Morales-Ruano, S., Morata, D., Boyce, A.J., Belmar, M., Fallick, A.E. and Hach-Alí, P.F. (2008) Mineralogy and geochemistry of El Dorado epithermal gold deposit, El Sauce district, central-northern Chile. *Mineralogy and Petrology*, **92**, 341–360.

Chetty, R., Bali, A. and Mallik, R.C. (2015) Tetrahedrites as thermoelectric materials: an overview. *Journal of Materials Chemistry C*, **3**, 12364–12378.

Ciobanu, C.L., Cook, N.J., Capraru, N., Damian, G. and Cristea, P. (2005) Mineral assemblages from the vein salband at Sacarimb, Golden Quadrilateral, Romania: I. Sulphides and sulphosalts. *Geokhimiia, Mineralogiia i Petrologiia*, **43**, 47–55.

Dimitrova, D., Kerestedjian, T., Petrova, M. and Iliev, T. (2007) Compositional variations in the tetrahedrite-

tennantite fahlores and polybasite-pearceite series from the Chiprovtsi Ag-Pb deposit, northwestern Bulgaria. *Proceedings of the 2007 Field Workshop of IGCP 486, Espoo, Finland, 26-31.08.2007*, 39–44.

Dittrich, H., Stadler, A., Topa, D., Schimper, H.-J. and Basch, A. (2009) Progress in sulfosalt research. *Physica Status Solidi (a)*, **206**, 1034–1041.

Douglass, R.M., Murphy, M.J. and Pabst, A. (1954) Geocronite. *American Mineralogist*, **39**, 908–928.

Edenharter, A. and Nowacki, W. (1970) Verfeinerung der Kristallstruktur von Bournonit [$(SbS_3)_2|Cu_2^{IV}Pb^{VII}Pb^{VIII}$] und von Seligmannit [$(AsS_3)_2|Cu_2^{IV}Pb^{VII}Pb^{VIII}$]. *Zeitschrift für Kristallographie – Crystalline Materials*, **131**, 397–417.

Fadda, S., Fiori, M. and Grillo, S.M. (2005) Chemical variations in tetrahedrite-tennantite minerals from the Furtei epithermal Au deposit, Sardinia, Italy: Mineral zoning and ore fluids evolution. *Geochemistry, Mineralogy and Petrology*, **43**, 79–84.

Foit, F.F. and Ulbricht, M.E. (2001) Compositional variation in mercurian tetrahedrite-tennantite from the epithermal deposits of the Steens and Pueblo Mountains, Harney County, Oregon. *Canadian Mineralogist*, **39**, 819–830.

Gemmell, J.B., Zantop, H. and Birnie, R.W. (1989) Silver sulfosalts of the Santo-Nino vein, Fresnillo district, Zacatecas, Mexico. *Canadian Mineralogist*, **27**, 401–418.

Hackbarth, C.J. and Petersen, U. (1984) A fractional crystallization model for the deposition of argentian tetrahedrite. *Economic Geology*, **79**, 448–460.

Johnson, N.E., Craig, J.R. and Rimstidt, J.D. (1986) Compositional trends in tetrahedrite. *Canadian Mineralogist*, **24**, 385–397.

Johnson, N.E., Craig, J.R. and Rimstidt, J.D. (1987) Effect of substitutions on the cell dimensions of tetrahedrite. *Canadian Mineralogist*, **25**, 237–244.

Johnson, N.E., Craig, J.R. and Rimstidt, J.D. (1988) Crystal-chemistry of tetrahedrite. *American Mineralogist*, **73**, 389–397.

Karup-Møller, S. and Makovicky, E. (2003) Exploratory studies of element substitutions in synthetic tetrahedrite. Part V. Mercurian tetrahedrite. *Neues Jahrbuch für Mineralogie, Abhandlungen*, **179**, 73–83.

Kharbish, S. (2011) Raman spectroscopic investigations of some Tl-sulfosalt minerals containing pyramidal $(As,Sb)S_3$ groups. *American Mineralogist*, **96**, 609–616.

Kharbish, S. (2016) Micro-Raman spectroscopic investigations of extremely scarce Pb-As sulfosalt minerals: baumhauerite, dufrénoysite, gratonite, sartorite, and seligmannite. *Journal of Raman Spectroscopy*, **47**, 1360–1366.

Kharbish, S. and Jeleň, S. (2016) Raman spectroscopy of the Pb-Sb sulfosalt minerals: boulangerite, jamesonite, robinsonite and zinkenite. *Vibrational Spectroscopy*, **85**, 157–166.

Kharbish, S., Götzinger, M. and Beran, A. (2007*a*) Compositional variations of fahlore group minerals from Austria. *Austrian Journal of Earth Science*, **100**, 44–52.

Kharbish, S., Libowitzky, E. and Beran, A. (2007*b*) The effect of As-Sb substitution in the Raman spectra of tetrahedrite-tennantite and pyrargyrite-proustite solid solutions. *European Journal of Mineralogy*, **19**, 567–574.

Kharbish, S., Libowitzky, E. and Beran, A. (2009) Raman spectra of isolated and interconnected pyramidal XS_3 groups (X = Sb,Bi) in stibnite, bismuthinite, kermesite, stephanite and bournonite. *European Journal of Mineralogy*, **21**, 325–333.

Kharbish, S., Giester, G. and Beran, A. (2010) Contribution to the crystal structures of tennantite and bournonite. *Neues Jahrbuch für Mineralogie, Abhandlungen*, **187**, 159–166.

Krismer, M., Vavtar, F., Tropper, P., Kaindl, R. and Sartory, B. (2011*a*) The chemical composition of tetrahedrite-tennantite ores from the prehistoric and historic Schwaz and Brixlegg mining areas (North Tyrol, Austria). *European Journal of Mineralogy*, **23**, 925–936.

Krismer, M., Vavtar, F., Tropper, P., Sartory, B. and Kaindl, R. (2011*b*) Mineralogy, mineral chemistry and petrology of the Ag-bearing Cu-Fe-Pb-Zn sulfide mineralizations of the Pfunderer Berg (South Tyrol, Italy). *Austrian Journal of Earth Sciences*, **104**, 36–48.

Lafuente, B., Downs, R., Yang, H. and Stone, N. (2015) The power of databases: the RRUFF project. *Highlights in Mineralogical Crystallography*, 1–30.

Makovicky, E. (1994) Exploratory studies on substitution of minor elements in synthetic tetrahedrite. Part I. Substitution by Fe, Zu, Co, Ni, Mn, Cr, V, and Pb. Unit cell parameter changes on substitution and the structural role of Cu*O_2*O+. *Neues Jahrbuch für Mineralogie, Abhandlungen*, **167**, 89–123.

Makovicky, E. and Skinner, B.J. (1978) Studies of the sulfosalts of copper. VI. Low-temperature exsolution in synthetic tetrahedrite solid solution, $Cu_{12+x}Sb_{4+y}S_{13}$. *Canadian Mineralogist*, **16**, 611–623.

Makovicky, E., Tippelt, G., Forcher, K., Lottermoser, W., Karup-Moller, S. and Amthauer, G. (2003) Mössbauer study of Fe-bearing synthetic tennantite. *Canadian Mineralogist*, **41**, 1125–1134.

Makovicky, E., Karanovic, L., Poleti, D., Balic-Zunic, T. and Paar, W.H. (2005) Crystal structure of copper-rich unsubstituted tennantite, $Cu_{12.5}As_4S_{13}$. *Canadian Mineralogist*, **43**, 679–688.

Miller, J.W. and Craig, J.R. (1983) Tetrahedrite tennantite series compositional variations in the Cofer Deposit,

https://doi.org/10.1180/minmag.2017.081.008 Published online by Cambridge University Press

Mineral District, Virginia. *American Mineralogist*, **68**, 227–234.

Minceva-Sukarova, B., Jovanovski, G., Makreski, P., Soptrajanov, B., Griffith, W., Willis, R. and Grzetic, I. (2003) Vibrational spectra of MIMIII S2 type synthetic minerals (MI = Tl or Ag and MIII = As or Sb). *Journal of Molecular Structure*, **651–653**, 181–189.

Moëlo, Y., Makovicky, E., Mozgova, N.N., Jambor, J.L., Cook, N., Pring, A., Paar, W., Nickel, E.H., Graeser, S., Karup-Møller, S., Balic-Žunic, T., Mumme, W.G., Vurro, F., Topa, D., Bindi, L., Bente, K. and Shimizu, M. (2008) Sulfosalt systematics: a review. Report of the sulfosalt sub-committee of the IMA Commission on Ore Mineralogy. *European Journal of Mineralogy*, **20**, 7–62.

Mohanan, K., Sharma, S.K. and Bishop, F.C. (1993) A Raman spectral study of forsterite-monticellite solid solutions. *American Mineralogist*, **78**, 42–48.

Nakamoto, K. (1997) *Infrared and Raman Spectra of Inorganic and Coordination Chemistry*. Wiley, New York.

Pattrick, R.A.D. and Hall, A.J. (1983) Silver substitution into synthetic zinc, cadmium, and iron tetrahedrites. *Mineralogical Magazine*, **47**, 441–451.

Repstock, A., Voudouris, P., Zeug, M., Melfos, V., Zhai, M., Li, H., Kartal, T. and Matuszczak, J. (2015) Chemical composition and varieties of fahlore-group minerals from Oligocene mineralization in the Rhodope area, southern Bulgaria and northern Greece. *Mineralogy and Petrology*, **110**, 103–123.

Rividi, N., van Zuilen, M., Philippot, P., Menez, B., Godard, G. and Poidatz, E. (2010) Calibration of carbonate composition using micro-Raman analysis: application to planetary surface exploration. *Astrobiology*, **10**, 293–309.

Sack, R.O. and Ebel, D.S. (1993) As-Sb exchange energies in tetrahedrite–tennantite fahlores and bournonite–seligmannite solid solutions. *Mineralogical Magazine*, **57**, 635–642.

Sack, R.O. and Loucks, R.R. (1985) Thermodynamic properties of tetrahedrite-tennantites – Constraints on the interdependence of the Ag-reversible-Cu, Fe-reversible-Zn, Cu-reversible-Fe, and As-reversible-Sb exchange-reactions. *American Mineralogist*, **70**, 1270–1289.

Skinner, B.J., Luce, F.D. and Makovicky, E. (1972) Studies of the sulfosalts of copper III; Phases and phase relations in the system Cu-Sb-S. *Economic Geology*, **67**, 924–938.

Takéuchi, Y. and Haga, N. (1969) On the crystal structures of seligmannite, $PbCuAsS_3$, and related minerals. *Zeitschrift für Kristallographie*, **130**, 254–260.

Vakh, A.S., Avchenko, O.V., Goryachev, N.A., Gvozdev, V.I. and Karabtsov, A.A. (2016) New data on the composition of jordanite–geocronite Pb–Sb–As sulfosalts at the Berezitovoe deposit (Upper Amur region, Russia). *Doklady Earth Sciences*, **467**, 402–407.

Vassileva, R.D., Atanassova, R. and Kouzmanov, K. (2013) Tennantite-tetrahedrite series from the Madan Pb-Zn deposits, Central Rhodopes, Bulgaria. *Mineralogy and Petrology*, **108**, 515–531.

Wang, A., Han, J.Y., Guo, L.H., Yu, J.Y. and Zeng, P. (1994) Database of standard Raman spectra of minerals and related inorganic crystals. *Applied Spectroscopy*, **48**, 959–968.

Wu, I. and Petersen, U. (1977) Geochemistry of tetrahedrite and mineral zoning at Casapalca, Peru. *Economic Geology*, **72**, 993–1016.

Wu, I.J. and Birnie, R.W. (1977) The bournonite-seligmannite solid solution. *American Mineralogist*, **62**, 1097–1100.

Wuensch, B.J. (1964) The crystal structure of tetrahedrite, $Cu_{12}Sb_4S_{18}$. *Zeitschrift für Kristallographie – Crystalline Materials*, **119**, 437–453.

https://doi.org/10.1180/minmag.2017.081.008 Published online by Cambridge University Press